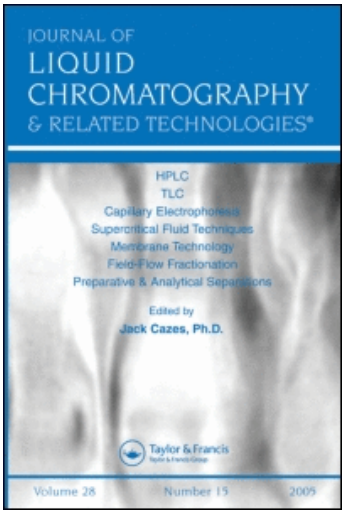

Journal of Liquid Chromatography & Related Technologies
Publication details, including instructions for authors and subscription information:
http://www.informaworld.com/smpp/title~content=t713597273

COMPARISON OF THEORETICAL METHODS FOR EXTRACTING RETENTION FACTORS AND RATE CONSTANTS IN LIQUID CHROMATOGRAPHY

Amber M. Hupp[a]; Victoria L. McGuffin[a]
[a] Department of Chemistry, Michigan State University, East Lansing, Michigan, USA

Online publication date: 01 October 2010

To cite this Article Hupp, Amber M. and McGuffin, Victoria L.(2010) 'COMPARISON OF THEORETICAL METHODS FOR EXTRACTING RETENTION FACTORS AND RATE CONSTANTS IN LIQUID CHROMATOGRAPHY', Journal of Liquid Chromatography & Related Technologies, 33: 15, 1427 — 1458
To link to this Article: DOI: 10.1080/10826076.2010.503785
URL: http://dx.doi.org/10.1080/10826076.2010.503785

Journal of Liquid Chromatography & Related Technologies, 33:1427–1458, 2010

ISSN: 1082-6076 print/1520-572X online
DOI: 10.1080/10826076.2010.503785

COMPARISON OF THEORETICAL METHODS FOR EXTRACTING RETENTION FACTORS AND RATE CONSTANTS IN LIQUID CHROMATOGRAPHY

Amber M. Hupp and Victoria L. McGuffin
Department of Chemistry, Michigan State University, East Lansing, Michigan, USA

□ *In this research, experimental data are used to evaluate theoretical methods that provide detailed information concerning mass transfer processes in liquid chromatography. To this end, a well-characterized homologous series of fatty acids is separated on a polymeric octadecyl silica stationary phase with a methanol mobile phase. These solutes are detected via laser-induced fluorescence to generate characteristic zone profiles as a function of column length and linear velocity. Three theoretical methods are then applied to extract the thermodynamic and kinetic information from the zone profiles. Each method relies on evaluating the shape of the zone profiles. The statistical moments of the profiles are used to calculate the mean and variance, which are related to the retention factor and rate constant, respectively. The profiles are also fit to the exponentially modified Gaussian equation and the Thomas equation. The fitting parameters from these equations are then used to calculate the retention factors and rate constants. These methods are compared and their inherent advantages and limitations are discussed.*

Keywords exponentially modified Gaussian function, kinetic rate constants, liquid chromatography, retention factor, statistical moments, Thomas model

INTRODUCTION

In order to deeply understand chromatographic and related separations, both thermodynamic and kinetic information are required.[1] Thermodynamic processes control the retention and selectivity, whereas kinetic processes control the extent of zone broadening and asymmetry, each of which affect the resolution of the separation. A number of studies have been performed to elicit thermodynamic behavior, which is now well understood for many systems.[2–5] However, kinetic behavior has not been studied in as much detail. The conditions of slow kinetics continue to exist

Address correspondence to Victoria L. McGuffin, Department of Chemistry, Michigan State University, East Lansing, Michigan 48824, USA. E-mail: jgshabus@aol.com

and need to be improved in liquid chromatography, particularly for adsorption, complexation, chiral, affinity, and ion exchange mechanisms.[3] Thus, a detailed understanding of kinetic behavior is necessary to identify the rate-limiting processes so that separation speed may be increased without sacrificing resolution. In order to better understand kinetic processes, accurate measurement of rate constants and the associated kinetic parameters must be accomplished.

A number of approaches have been used to determine kinetic parameters.[3] Most commonly, direct chromatographic approaches are utilized, where the zone profile is extracted from the elution chromatogram and then analyzed by different methods. Of these, the plate height method is the most commonly used.[6–9] In this method, the zone profile is analyzed to determine the plate height, either from the width or the variance, which is then related to the rate constants for mass transport. Another common method is the exponentially modified Gaussian (EMG) model.[10,11] By fitting the zone profiles to the EMG function, McGuffin et al. were able to extract the kinetic properties arising from slow kinetics of mass transfer.[12–15] Other models for studying thermodynamic and kinetic behavior include those developed by Giddings,[1] by Haarhoff and van der Linde,[16] and by Thomas.[17,18] The Giddings model can be employed for single-site adsorption under linear isotherm conditions, whereas the Haarhoff–van der Linde and Thomas models can be used under linear or nonlinear isotherm conditions. These models have many applications in reversed-phase,[14,15,19] adsorption,[20,21] and affinity[20,22] chromatography.

To date, there have been few studies that directly compare and validate theoretical methods for extracting kinetic parameters from chromatographic data. Using stochastic simulation, Li and McGuffin evaluated several methods for extracting kinetic rate constants by comparison to the "true" value.[23] While each method had advantages and limitations, each was found capable of determining thermodynamic and kinetic parameters accurately under the ideal conditions specified in the stochastic simulation. However, the ability of these methods to extract thermodynamic and kinetic information under practical conditions, where column and extra-column contributions affect broadening and asymmetry, remains to be evaluated.

The goals of this research are as follows: (1) to generate experimental zone profiles as a function of column length, mobile phase linear velocity, and solute carbon number; (2) to extract retention factors and kinetic rate constants using different theoretical methods; and (3) to compare each method with respect to their advantages and limitations. The experimental conditions are specifically chosen to facilitate these goals. A well-characterized homologous series is separated on an octadecyl silica stationary phase that provides a wide range of retention factors and rate constants.

In this manner, the theoretical methods can be compared for well-behaved solutes as well as those undergoing slow kinetic processes.

THEORY

The retention factor is a thermodynamic description of the interaction strength of a solute with the mobile and stationary phases. The retention factor (k) is calculated from measurable chromatographic parameters by

$$k = \frac{t_r - t_0}{t_0} \tag{1}$$

where t_r is the retention time of the solute and t_0 is the elution time of a non-retained compound. The kinetic rate constants quantify kinetic aspects of the rate of solute transfer, and are related to the retention factor by

$$k = \frac{k_{sm}}{k_{ms}} \tag{2}$$

where k_{sm} is the rate constant for the transfer from mobile to stationary phase and k_{ms} is the rate constant for the transfer from stationary to mobile phase.

Statistical Moment Method

In the statistical moment method, the moments may be calculated directly from the zone profiles (i.e., without regression to specific equations). The first and second statistical moments in time units are defined as

$$M_1 = \frac{\int C(t)t\,dt}{\int C(t)\,dt} \tag{3}$$

$$M_2 = \frac{\int C(t)(t - M_1)^2\,dt}{\int C(t)\,dt} \tag{4}$$

where C(t) is the solute concentration as a function of time, M_1 is the mean retention time, and M_2 is the peak variance. The retention factor is determined from the first moment by

$$k = \frac{M_1 - t_0}{t_0} \tag{5}$$

The method of calculating kinetic rate constants is derived by extension of Giddings' work.[1] The plate height (H) can be related to the second moment by

$$H = \frac{M_2 L}{M_1^2} \tag{6}$$

where L is the column length. The mass transfer term (C_s) for slow kinetics is given by

$$C_s = \frac{2k}{(1+k)^2 k_{ms}} \tag{7}$$

Thus, the rate constants are related to the plate height by

$$k_{ms} = \frac{2ku}{(1+k)^2 \Delta H} \quad \text{and} \quad k_{sm} = \frac{2k^2 u}{(1+k)^2 \Delta H} \tag{8}$$

where u is the linear velocity and ΔH is the corrected plate height. The corrected plate height represents slow mass transfer in the stationary phase (C_s), and is calculated by

$$\Delta H = C_s u = H - A - \frac{B_m}{u} - \frac{B_s}{u} - C_m u \tag{9}$$

where A, B_m, B_s, and C_m are the classical contributions to zone broadening.[1] The multiple paths term (A) characterizes the broadening that arises from the variety of flow paths available in the packed column, and is given by

$$A = 2\lambda d_p \tag{10}$$

where λ is the packing factor and d_p is the particle size. The longitudinal diffusion terms (B_m and B_s) characterize the random motion of molecules in the mobile and stationary phases, respectively, and are given by

$$B_m = 2\gamma_m D_m \tag{11}$$

$$B_s = 2\gamma_s D_s k \tag{12}$$

where γ_m and γ_s are obstruction factors and D_m and D_s are the diffusion coefficients of the solute in the mobile and stationary phases, respectively. The resistance to mass transfer term (C_m) represents broadening that arises because solute molecules tend to remain in the same flow stream,

each of which has a different velocity. This contribution is given by van Deemter[24] as

$$C_m = \frac{k^2 d_p^2}{100(1+k)^2 D_m} \tag{13}$$

The van Deemter form was chosen because it requires no empirical parameters and it performed more consistently in this study than the Purnell,[25] Giddings,[1] and Giddings coupling[26,27] equations, as well as the Miyabe-Guiochon method.[9] The evaluation of these equations is discussed in detail in the Appendix.

As shown in Equation (9), each of the broadening contributions in Equations (10) to (13) is subtracted from the plate height in order to give the corrected plate height. However, each contribution includes a parameter that is based on estimation. For this study, λ, γ_m, and γ_s are taken as unity, D_m is on the order of $10^{-5}\,cm^2\,s^{-1}$ and D_s ranges from 10^{-6} to $10^{-9}\,cm^2\,s^{-1}$ for solutes C_{10} to C_{20}, which were estimated using the Wilke-Chang equation.[28]

Statistical moments are an accurate method of determining the broadening or plate height because they make no assumptions regarding the shape of the solute zone. The model assumes that all contributions to variance that are not directly attributable to fast processes, such as axial dispersion, arise from slow kinetics. Implicitly, this suggests that slow kinetics arises in the stationary phase. For a traditional packed column with a partition mechanism, this may include external mass transfer, intraparticle diffusion, and sorption/desorption kinetics.[9] There are several potential sources of error in this method. The solute concentration must be within the linear region of the isotherm, so that it does not contribute to the variance. Additionally, accurate calculation and subtraction of all fast mass transfer terms (A, B_m, B_s, and C_m) must be performed, which is problematic for packed columns in liquid chromatography. Empirical estimations of these parameters will introduce errors. Finally, any extra-column contributions to broadening, including those from the injector, detector, connections, etc., must be minimized or eliminated to assure accurate calculation of thermodynamic and kinetic parameters. Since there are no theoretical methods for the calculation of these parameters, empirical estimations are necessary. In this work, extra-column contributions are eliminated by detection at several points along the chromatographic column, with subtraction of the parameters determined at each detector. Thus, Equations (5) and (6) become

$$k = \frac{\Delta M_1 - \Delta t_0}{\Delta t_0} \tag{14}$$

$$H = \frac{\Delta M_2 \Delta L}{(\Delta M_1)^2} \tag{15}$$

where Δt_0 is the difference in the elution time of a non-retained species, ΔM_1 is the difference in the first moment, ΔM_2 is the difference in the second moment, and ΔL is the distance between two on-column detectors.

Exponentially Modified Gaussian Method

When an incremental length of the chromatographic column is considered, the zone broadening processes described in Equations (10) to (13) are fast relative to the time spent in the incremental length. These processes contribute to the symmetric broadening, which is described by a Gaussian function

$$C(t) = \frac{A}{\sqrt{2\pi}\sigma_g} \exp\left(-0.5\left(\frac{t - t_g}{\sigma_g}\right)^2\right) \tag{16}$$

where A is the area, t_g is the retention time of the Gaussian component, and σ_g is the standard deviation of the Gaussian component. Zone broadening can also arise from mass transfer processes that are slow relative to the time spent in the incremental length. These processes contribute to the asymmetric broadening. For a partition or adsorption mechanism considered as a first-order or pseudo-first-order reaction, this contribution is given by an exponential function

$$C(t) = A \exp\left(\frac{-(t - t_g)}{\tau}\right) \tag{17}$$

where τ is the standard deviation of the exponential component.

The resulting zone profile is the convolution of the Gaussian and the exponential contributions, which is given by the exponentially modified Gaussian (EMG) equation

$$C(t) = \frac{A}{2\tau} \exp\left(\frac{\sigma_g^2}{2\tau^2} + \frac{t_g - t}{\tau}\right)\left(\operatorname{erf}\left(\frac{t - t_g}{\sqrt{2}\sigma_g} - \frac{\sigma_g}{\sqrt{2}\tau}\right) + 1\right) \tag{18}$$

The zone profile is fit to the EMG equation by nonlinear regression to extract the regression parameters. From these parameters, the retention

time (t_r) is calculated as

$$t_r = t_g + \tau \tag{19}$$

and the corresponding retention factor is calculated from Equation (1).

The method of calculating kinetic rate constants from the EMG model is derived by extension of Giddings' work.[1,13] The mass transfer term for slow kinetics is given by Equation (7). By rearrangement, the rate constants are given by:

$$k_{ms} = \frac{2kt_0}{\tau^2} \quad \text{and} \quad k_{sm} = \frac{2k^2 t_0}{\tau^2} \tag{20}$$

This method of determining the rate of transfer between phases by adjusting an exponential equation on the tail of an asymmetric peak has been justified by Vidal-Madjar and Guiochon,[29] and applied extensively by McGuffin et al.[12–15,23]

In the EMG method, thermodynamic parameters are calculated using both symmetric and asymmetric portions of the peak, while the kinetic parameters are calculated using only the asymmetric portion of the peak. This model assumes that all the contributions to asymmetric broadening (τ) arise from slow kinetics. There are several potential sources of error in this method. The solute concentration must be within the linear region of the isotherm, so that it does not contribute to the asymmetry. In addition, any extra-column contributions to asymmetry must be minimized or eliminated. In this work, this is accomplished by detection at several points along the chromatographic column, with subtraction of the parameters determined at each detector. Thus, Equations (1) and (20) become

$$k = \frac{\Delta t_r - \Delta t_0}{\Delta t_0} \tag{21}$$

$$k_{ms} = \frac{2k\Delta t_0}{\Delta\tau^2} \quad \text{and} \quad k_{sm} = \frac{2k^2\Delta t_0}{\Delta\tau^2} \tag{22}$$

where Δt_r is the difference in the retention time and $\Delta\tau^2$ is the difference in τ^2. The EMG model is especially useful as it does not require *a priori* estimation of symmetric column or extra-column contributions to broadening.

Thomas Method

A method for extracting thermodynamic and kinetic information for frontal profiles was reported by Thomas[18] and later modified for elution

zone profiles by Wade et al.[17] This model was derived for mechanisms that can be considered as second-order sorption and first-order desorption reactions under linear and nonlinear conditions. This theoretical equation is given by

$$C(x) = \frac{A\gamma}{KC_0}(1 - \exp(-\gamma KC_0))\left(\frac{\sqrt{k/x}I_1(2\gamma\sqrt{kx})\exp(-\gamma x - \gamma k)}{1 - T(\gamma k, \gamma x)(1 - \exp(-\gamma KC_0))}\right) \quad (23)$$

where

$$T(u, v) = \exp(-v)\int_0^u \exp(-x)I_0(\sqrt{2vx})\mathrm{dx} \quad (24)$$

and A is the area, γ is a dimensionless constant equal to the product of the desorption rate constant (k_{ms}) and t_0, K is the equilibrium constant, k is the mean, and C_0 is the initial concentration. After conversion from the time domain (t) to the retention factor domain (x), the zone profile is fit by nonlinear regression to Equation (23). From the regression parameters (A, k, γ, KC_0), the corresponding retention factor and rate constants are obtained.

The Thomas model assumes that all contributions to symmetric and asymmetric broadening arise from nonlinear isotherms and slow kinetics. There are several potential sources of error in the method. First, the method assumes the kinetics and the isotherm to be Langmuirian. Next, column contributions from multiple paths and diffusion in the mobile and stationary phases must be negligible. Additionally, any extra-column contributions, including those from the injector, detector, connections, etc., must also be negligible. However, unlike the moment and EMG models, there is no *a posteriori* method to correct for these contributions.

EXPERIMENTAL METHODS

Chemicals

A series of fatty acids (Sigma) ranging from C_{10} to C_{20} is derivatized with 4-bromomethyl-7-methoxycoumarin (Sigma), as described previously.[30] The solvent is evaporated in a stream of dry nitrogen at 40°C and the residue is dissolved in high-purity methanol (Burdick and Jackson Division, Honeywell).

Experimental System

The solutes are separated by capillary liquid chromatography. A fused-silica capillary (200 μm i.d., 76 cm, Polymicro Technologies) is packed

via the slurry method and terminated with a quartz wool frit. The packing material is a polymeric octadecyl silica phase that is characterized by a 5.5 μm particle size, 190 Å pore size, and 240 $m^2 g^{-1}$ surface area (IMPAQ 200, PQ Corp.). It is prepared by reaction of the silica support with triethoxyoctadecylsilane at a bonding density of 5.4 μmol m^{-2}. Columns prepared in this manner have uniform radial and axial packing and have small extra-column variance, on the order of 10 nL.[31]

The methanol mobile phase (Burdick and Jackson Division, Honeywell) is delivered via a single-piston reciprocating pump (Model 114 M, Beckman Instruments) that is operated in constant-pressure mode at 4000 psi. The sample is introduced by a 1.0 μL injection valve (Model ECI4W1, Valco Instruments) and then is split between the capillary column and a fused-silica capillary (50 μm i.d., 60 cm, Polymicro Technologies). Another fused-silica capillary (20 μm i.d., 2000 cm, Polymicro Technologies) is attached post-column to serve as a restrictor. The length of the restrictor is systematically decreased to adjust the flow rate along the column while maintaining constant pressure. The injector, splitter, column, and restrictor are enclosed within a cryogenic oven maintained at 30°C.

Solute detection is achieved by on-column laser-induced fluorescence.[31] A continuous-wave helium-cadmium laser (Model 3074–20 M, Melles Griot), with approximately 28 mW power at 325 nm, is used as the excitation source. The laser is focused onto UV-grade optical fibers (100 μm, Polymicro Technologies) and is transmitted to four locations along the column (23.2, 28.7, 52.8, 58.3 cm) where the polyimide coating on the capillary has been removed. The fluorescence power at each location is collected orthogonally by large diameter optical fibers (500 μm, Polymicro Technologies) and transmitted through a 420-nm interference filter (S10-410-F, Corion) to a photomultiplier tube (Model R760, Hamamatsu). After amplification, the photocurrent is converted to the digital domain (PCI-MIO-16XE-50, National Instruments) and stored by a user-defined program (Labview v5.1, National Instruments).

Data Analysis

After separation, the solute zone profiles are individually extracted from the chromatogram and then analyzed. In preliminary studies, several models were examined for experimental data analysis. Each profile was fit by nonlinear regression to the Gaussian and Giddings equations by a commercially available program (PeakFit v4.14, SYSTAT Software). The Gaussian model assumes a symmetric peak shape, whereas the Giddings model assumes negligible column contributions from multiple paths and diffusion in the mobile and stationary phases; both assumptions are not valid for all solutes in this experiment. The Gaussian model produced

nonrandom residuals with correlation coefficients ranging from 0.990 to 0.813 for C_{10} to C_{20}, respectively. The Giddings model also contained nonrandom residuals with correlation coefficients ranging from 0.990 to 0.830 for C_{10} to C_{20}, respectively. Due to the poor quality of fit, these models were not used for further analysis of the zone profiles. Other models that can account for asymmetric peak shapes were then evaluated and determined to be more suitable. For the statistical moment method, the profile was fit to an asymmetric double sigmoidal function (ADS), using a commercially available program (TableCurve v2.02, SYSTAT Software). The fit equation was then regenerated (Excel v2003, Microsoft), from which the statistical moments are calculated. This method produces high quality fits (correlation coefficients ranging from 0.999 to 0.979), reduces noise, and allows control of peak integration limits. In this work, the integration limits are identified at 0.1% of the maximum peak height, as the error in the statistical moments, particularly the second moment, has been proven small under these conditions.[32] Each profile is also fit by nonlinear regression to the EMG and Thomas equations by a commercially available program (PeakFit v4.14, SYSTAT Software). The regression of the zone profiles to each of these equations is excellent, with correlation coefficients ranging from 0.999 to 0.941 for the EMG equation and 0.998 to 0.942 for the Thomas equation. However, each of the models fits the zone profile differently. As shown in Figure 1, the EMG model overestimates the peak maximum and tail and underestimates the region around the mean, while the Thomas model behaves in the opposite manner. The high correlation

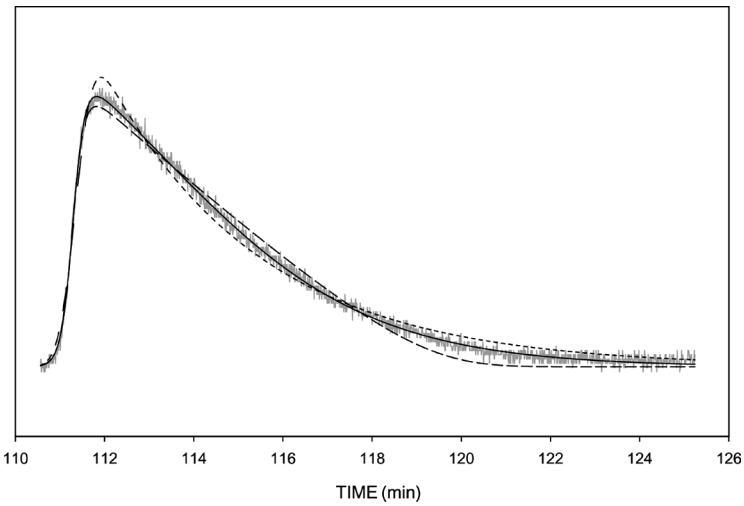

FIGURE 1 Regression analysis of coumarin-labeled C_{18} fatty acid at 0.062 cm s^{-1}. Experimental data (—), exponentially modified Gaussian equation (----), Thomas equation (— —), asymmetric double sigmoidal equation (——).

coefficients result from the average of positive and negative error in both the EMG and Thomas models. The fit of the ADS equation is most accurate; however, it lacks physical and chromatographic significance.

RESULTS AND DISCUSSION

Retention Factor

The retention factors at each on-column detector at a representative linear velocity are plotted in Figure 2. The trends shown here are observed consistently at each linear velocity. These retention factors are not corrected for extra-column effects. For all methods, the retention factor increases slightly as a function of column length. For example, if the C_{16} fatty acid is considered, the retention factor increases by 4.8% for the statistical moment, 4.6% for the EMG, and 3.5% for the Thomas methods. To further examine the effect of distance on retention factor, the difference method was used, as it corrects for volume- and time-based extra-column variance.[31] The retention factors are calculated using Equation (21) between detectors 4 and 1 ($\Delta L = 35.1$ cm), detectors 4 and 2 ($\Delta L = 29.6$ cm), and detectors 3 and 2 ($\Delta L = 24.1$ cm), as summarized for the EMG model in Table 1. As the distance between the detectors increases, there is no significant change in the retention factor (0 to 1.4%). Because the retention factor is a measure of thermodynamic conditions, the constancy along the column implies that steady state has been achieved, and reliable extraction of the kinetic information can occur.

Representative values for the retention factor calculated by difference (between detectors 4 and 1) are summarized for each model in Tables 2–4. Retention factors are quite similar for all models and show the same trends with velocity and carbon number. The retention factor decreases with increasing linear velocity for all solutes. It may be noted that, at any velocity, the solute must transfer between the stationary and mobile phases toward equilibrium. At higher velocities, equilibrium conditions are more difficult to achieve because the mobile phase is moving faster, yet the stationary phase remains immobile, which leads to a decrease in retention. This effect is most apparent for solutes with longer alkyl chains, which on average spend a longer time in the stationary phase. For example, when using the statistical moment model, the retention factor for C_{10} decreases by approximately 13%, whereas the retention factor for C_{20} decreases by approximately 26% as the velocity is increased. Thus, a change in linear velocity plays a more significant role in the retention of solutes that are highly retained.

The retention factor increases logarithmically with an increase in carbon number, as shown in Figure 3. Each additional ethylene group

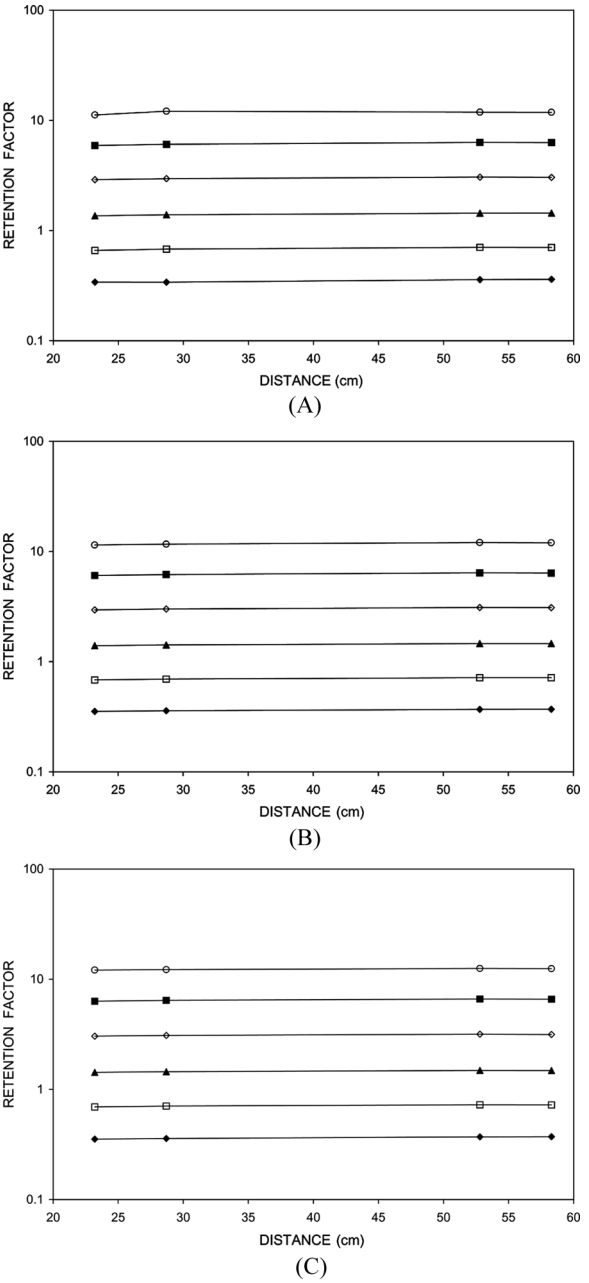

FIGURE 2 Retention factor plotted versus distance for statistical moment (A), exponentially modified Gaussian (B), and Thomas (C) methods at 0.088 cm s^{-1}. Solutes: C_{10} (◆), C_{12} (□), C_{14} (▲), C_{16} (◇), C_{18} (■), C_{20} (○).

TABLE 1 Retention Factors as a Function of Length (L) between Detectors Calculated using Exponentially Modified Gaussian Method at a Linear Velocity of 0.088 cm s^{-1}

	Retention Factor, k		
Solute	L4 – L1 = 35.1 cm	L4 – L2 = 29.6 cm	L3 – L2 = 24.1 cm
C_{10}	0.38	0.38	0.38
C_{12}	0.74	0.74	0.74
C_{14}	1.50	1.50	1.51
C_{16}	3.19	3.18	3.21
C_{18}	6.60	6.58	6.67
C_{20}	12.4	12.4	12.5

systematically adds to the interaction of the solute with the stationary phase, causing the solute to become more retained as the carbon number increases. The retention factors for each solute calculated with each model are within 3% of one another at all velocities, except the Thomas model at the highest velocity. At 0.368 cm s^{-1}, values for the Thomas model differ by 0 to 9.4% from those for the moment and EMG models. Overall, each model provides reasonably consistent thermodynamic information.

Rate Constant

While retention factors provide information about the equilibrium or steady-state chromatographic behavior, rate constants provide information about the non-equilibrium or kinetic behavior. The rate of mass transfer depends not only on the chemical structure of the solute, but also on the experimental conditions. For this reason, the distance the solute has traveled along the column, the velocity of the mobile phase, and the chemical structure of the solute are important with regard to their impact on the rate constants.

TABLE 2 Retention Factors for Coumarin-labeled Fatty Acids as a Function of Linear Velocity (u) using Statistical Moment Method by Difference Between Detectors 4 and 1

	Retention Factor, k				
Solute	u = 0.045 cm s^{-1}	u = 0.062 cm s^{-1}	u = 0.088 cm s^{-1}	u = 0.150 cm s^{-1}	u = 0.368 cm s^{-1}
C_{10}	0.39	0.39	0.38	0.37	0.34
C_{12}	0.76	0.75	0.74	0.71	0.64
C_{14}	1.55	1.53	1.51	1.43	1.21
C_{16}	3.30	3.27	3.18	2.99	2.41
C_{18}	6.85	6.79	6.58	6.12	4.69
C_{20}	12.9	12.8	12.3	11.5	8.52

TABLE 3 Retention Factors for Coumarin-labeled Fatty Acids as a Function of Linear Velocity (u) using Exponentially Modified Gaussian Method by Difference between Detectors 4 and 1

	Retention Factor, k				
Solute	$u = 0.045\,cm\,s^{-1}$	$u = 0.062\,cm\,s^{-1}$	$u = 0.088\,cm\,s^{-1}$	$u = 0.150\,cm\,s^{-1}$	$u = 0.368\,cm\,s^{-1}$
C_{10}	0.39	0.39	0.38	0.37	0.34
C_{12}	0.76	0.75	0.74	0.71	0.63
C_{14}	1.56	1.54	1.50	1.43	1.21
C_{16}	3.34	3.28	3.19	2.99	2.41
C_{18}	6.95	6.81	6.60	6.15	4.70
C_{20}	13.2	12.9	12.4	11.5	8.6

TABLE 4 Retention Factors for Coumarin-labeled Fatty Acids as a Function of Linear Velocity (u) using Thomas Method at Detector 4

	Retention Factor, k				
Solute	$u = 0.045\,cm\,s^{-1}$	$u = 0.062\,cm\,s^{-1}$	$u = 0.088\,cm\,s^{-1}$	$u = 0.150\,cm\,s^{-1}$	$u = 0.368\,cm\,s^{-1}$
C_{10}	0.38	0.37	0.37	0.36	0.34
C_{12}	0.74	0.73	0.72	0.71	0.65
C_{14}	1.51	1.50	1.48	1.42	1.27
C_{16}	3.25	3.22	3.15	3.01	2.57
C_{18}	6.78	6.72	6.58	6.23	5.11
C_{20}	12.9	12.8	12.5	11.8	9.49

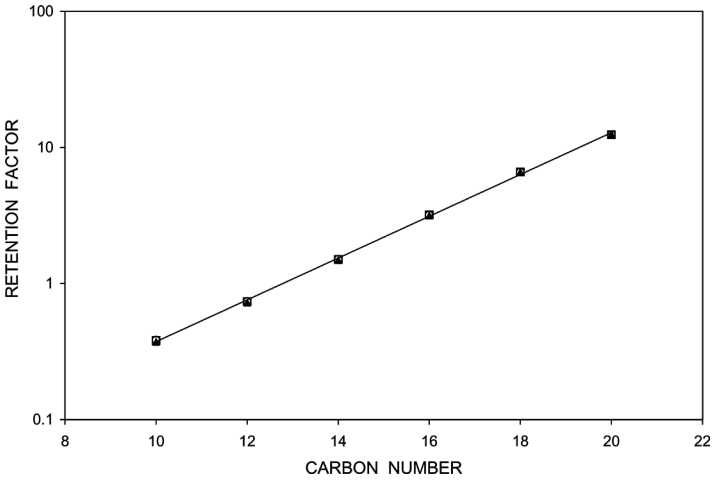

FIGURE 3 Retention factor plotted versus carbon number for statistical moment (○), exponentially modified Gaussian (□), and Thomas (▲) methods at $0.088\,cm\,s^{-1}$.

Effect of Column Length

If the system is at steady state, both the thermodynamic and kinetic properties should remain constant with distance. The preceding investigation of retention factor suggests that steady state has been achieved. Thus, the kinetic rate constants should be constant with distance as well. The rate constants from stationary to mobile phase (k_{ms}) at each on-column detector at a representative linear velocity are plotted in Figure 4. The trends shown here are observed consistently at each linear velocity. These rate constants are not corrected for extra-column effects. Obvious differences in the values for the rate constants using the three methods can be observed. First, rate constants for the statistical moment model fluctuate with increasing column length (Figure 4A), while they decrease slightly for the EMG model (Figure 4B), and are constant for the Thomas model (Figure 4C). In addition, the rate constants for C_{10} to C_{20} in the moment and EMG models span several orders of magnitude, while in the Thomas model they span only one order of magnitude. Moreover, rate constants fluctuate by as much as 86% for the moment method, 48% for the EMG method, and 39% for the Thomas method.

To investigate the effect of distance on the rate constants in more detail, the difference method was utilized. The rate constants are calculated using Equation (22) between detectors 4 and 1 ($\Delta L = 35.1$ cm), detectors 4 and 2 ($\Delta L = 29.6$ cm), and detectors 3 and 2 ($\Delta L = 24.1$ cm), as summarized for the EMG method in Table 5. As the distance between detectors increases, there is fluctuation in the rate constant for each solute (3 to 20%). This decrease in the amount of fluctuation, relative to 48% at an individual detector (*vide supra*), illustrates the advantage of using the difference method. Moreover, it is apparent that the moment and EMG methods by difference have less error than the Thomas method at a single detector. All methods show significant fluctuation, which suggests that these measurements should be considered, at best, an order of magnitude estimate of kinetic behavior.

Effect of Linear Velocity

Representative values for rate constants as a function of linear velocity are summarized in Tables 6–8. Both rate constants (k_{sm} and k_{ms}) calculated using each of the models show an overall increase with an increase in velocity. Bujalski experimentally investigated the diffusion-film thickness around an octadecyl silica particle using the shallow-bed technique.[33,34] As the flow rate was increased from 2.2 to 3.9 cm s^{-1}, the diffusion-film thickness decreased from 0.51 to 0.44 μm. If the stagnant mobile phase layer is thinner at higher velocities, the solute may be able to traverse through the layer faster. This suggests that a decrease in the thickness of

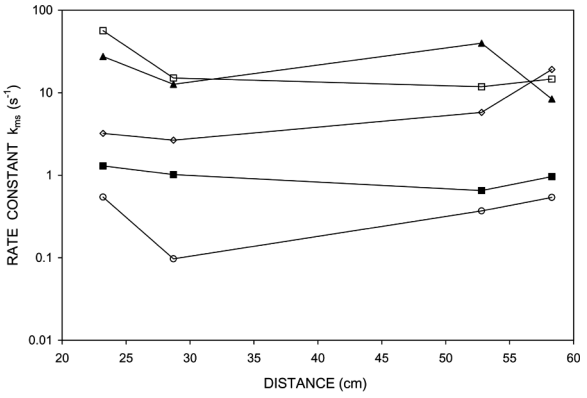

(A)

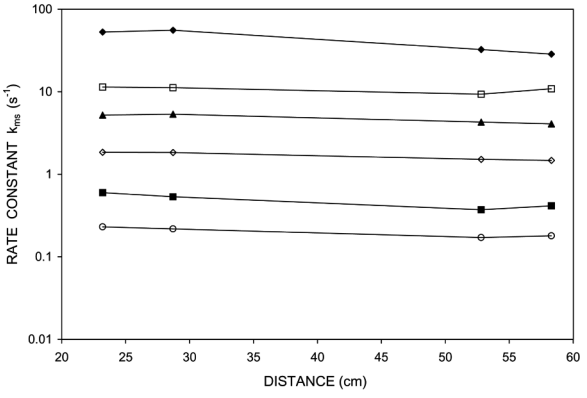

(B)

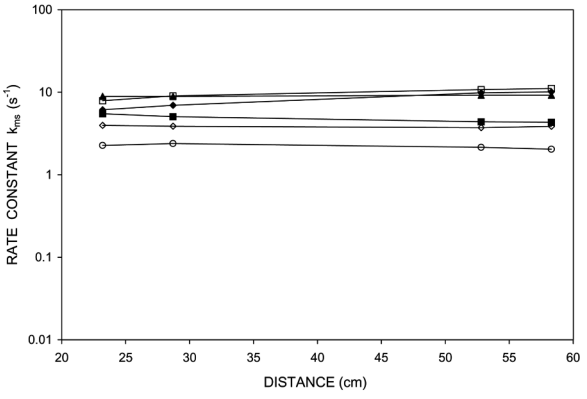

(C)

FIGURE 4 Rate constant plotted versus distance for statistical moment (A), exponentially modified Gaussian (B), and Thomas (C) methods at 0.088 cm s^{-1}. Solutes: C_{10} (◆), C_{12} (□), C_{14} (▲), C_{16} (◇), C_{18} (■), C_{20} (○).

TABLE 5 Rate Constants Calculated as a Function of Length (L) between Detectors using Exponentially Modified Gaussian Method at a Linear Velocity of 0.088 cm s^{-1}

	Rate Constant, k_{ms} (s^{-1})			Rate Constant, k_{sm} (s^{-1})		
Solute	L4 – L1 = 35.1 cm	L4 – L2 = 29.6 cm	L3 – L2 = 24.1 cm	L4 – L1 = 35.1 cm	L4 – L2 = 29.6 cm	L3 – L2 = 24.1 cm
C_{10}	22	19.5	26.9	8.4	7.4	10.2
C_{12}	11	10.6	9.7	7.8	7.8	7.2
C_{14}	3.6	3.3	4.3	5.3	5.0	6.5
C_{16}	1.3	1.2	1.5	4.1	3.9	5.0
C_{18}	0.35	0.34	0.34	2.3	2.3	2.3
C_{20}	0.16	0.15	0.17	1.9	1.9	2.1

the stagnant mobile phase layer surrounding the particle could cause k_{ms} and k_{sm} to increase with velocity, as observed in the present study.

Although the rate constants calculated using each of the three models show the same overall trends, their magnitude varies. For example, if k_{ms} for the C_{16} fatty acid is considered, values range from 0.98 to 4.7 s^{-1} for the statistical moment model, from 0.45 to 4.1 s^{-1} for the EMG model, and from 2.7 to 9.6 s^{-1} for the Thomas model for a linear velocity range of 0.045 cm s^{-1} to 0.368 cm s^{-1}. If k_{sm} for the same solute is then examined, values range from 3.2 to 11 s^{-1} for the moment model, from 1.5 to 9.9 s^{-1} for the EMG model, and from 8.9 to 25 s^{-1} for the Thomas model.

The observed differences in rate constants demonstrate the intrinsic capabilities and limitations of each model. For instance, rate constants for the C_{10} fatty acid could not be obtained at most velocities using the moment method. In this method, the rate constants are calculated directly from ΔH, the corrected plate height. If the sum of the theoretical A, B, and C terms is larger than the observed plate height, an overcorrection will occur that causes ΔH and the rate constants to be negative and, thus, indeterminate. This is common for very narrow peaks, where the theoretical correction terms overestimate the width of the experimental zone profile. This effect is an outcome and ultimate limitation of the statistical moment model. Additionally, several assumptions of the Thomas model limit its ability to calculate accurately the kinetic rate constants. First, as stated previously, the model assumes that all contributions to broadening arise from nonlinear isotherms and slow kinetics of adsorption/desorption. However, the concentrations used in this study are well within the linear region of the isotherm and the mechanism of retention is purely partition. Second, the method assumes that column contributions to variance from multiple paths and diffusion are negligible. However, in a packed column, these processes will be present and most assuredly will affect the peak broadening. Last, it should also be noted that the rate constants from the Thomas model are

TABLE 6 Rate Constants for Coumarin-labeled Fatty Acids as a Function of Linear Velocity (u) using Statistical Moment Method by Difference between Detectors 4 and 1

	Rate Constant, k_{ms} (s^{-1})					Rate Constant, k_{sm} (s^{-1})				
Solute	u = 0.045 cm s^{-1}	u = 0.062 cm s^{-1}	u = 0.088 cm s^{-1}	u = 0.150 cm s^{-1}	u = 0.368 cm s^{-1}	u = 0.045 cm s^{-1}	u = 0.062 cm s^{-1}	u = 0.088 cm s^{-1}	u = 0.150 cm s^{-1}	u = 0.368 cm s^{-1}
C_{10}	–	–	–	–	43	–	–	–	–	15
C_{12}	16	9.7	13	15	50	12	7.3	9.8	11	32
C_{14}	3.6	4	3.6	6.2	18	5.6	6.1	5.5	8.8	22
C_{16}	0.98	1.3	2.5	2.6	4.7	3.2	4.2	8.1	7.9	11
C_{18}	0.25	0.40	0.67	0.85	2.9	1.7	2.7	4.4	5.2	13
C_{20}	0.13	0.16	0.26	0.32	1.0	1.6	2.1	3.2	3.7	8.6

TABLE 7 Rate Constants for Coumarin-labeled Fatty Acids as a Function of Linear Velocity (u) using Exponentially Modified Gaussian Method by Difference between Detectors 4 and 1

	Rate Constant, k_{ms} (s^{-1})					Rate Constant, k_{sm} (s^{-1})				
Solute	u = 0.045 cm s^{-1}	u = 0.062 cm s^{-1}	u = 0.088 cm s^{-1}	u = 0.150 cm s^{-1}	u = 0.368 cm s^{-1}	u = 0.045 cm s^{-1}	u = 0.062 cm s^{-1}	u = 0.088 cm s^{-1}	u = 0.150 cm s^{-1}	u = 0.368 cm s^{-1}
C_{10}	17	19	22	65	–	6.7	7.4	8.4	24	–
C_{12}	5.4	6	11	15	24	4.1	4.5	7.8	11	15
C_{14}	1.8	2.8	3.6	6.9	12	2.9	4.3	5.3	9.8	15
C_{16}	0.45	1.0	1.3	2.0	4.1	1.5	3.4	4.1	5.9	9.9
C_{18}	0.11	0.23	0.35	0.47	1.6	0.78	1.5	2.3	2.9	7.4
C_{20}	0.05	0.09	0.16	0.17	0.49	0.68	1.2	1.9	2	4.2

TABLE 8 Rate Constants for Coumarin-labeled Fatty Acids as a Function of Linear Velocity (u) using Thomas Method at Detector 4

	Rate Constant, k_{ms} (s^{-1})					Rate Constant, k_{sm} (s^{-1})				
Solute	u = 0.045 cm s^{-1}	u = 0.062 cm s^{-1}	u = 0.088 cm s^{-1}	u = 0.150 cm s^{-1}	u = 0.368 cm s^{-1}	u = 0.045 cm s^{-1}	u = 0.062 cm s^{-1}	u = 0.088 cm s^{-1}	u = 0.150 cm s^{-1}	u = 0.368 cm s^{-1}
C_{10}	8.5	9.6	10	13	13	3.2	3.6	3.7	4.7	4.4
C_{12}	9.1	10	11	13	18	6.7	7.5	8.1	9.0	12
C_{14}	7.5	8.3	9.2	12	17	11	12	14	17	22
C_{16}	2.7	3.1	3.9	4.9	9.6	8.9	10	12	15	25
C_{18}	3.1	3.7	4.3	5.8	10	21	25	28	36	52
C_{20}	1.5	1.7	2.0	2.6	5.0	19	22	25	31	47

given only at the last on-column detector, while the moment and EMG models are calculated by taking the difference between the first and last detector. There is no direct way to use the difference approach with the Thomas model. Thus, any values calculated from the Thomas model inherently include extra-column contributions, which could lead to incorrect values for both thermodynamic and kinetic parameters.

Effect of Carbon Number

The rate of transfer between mobile and stationary phases is controlled by several factors related to the solute structure and properties. These

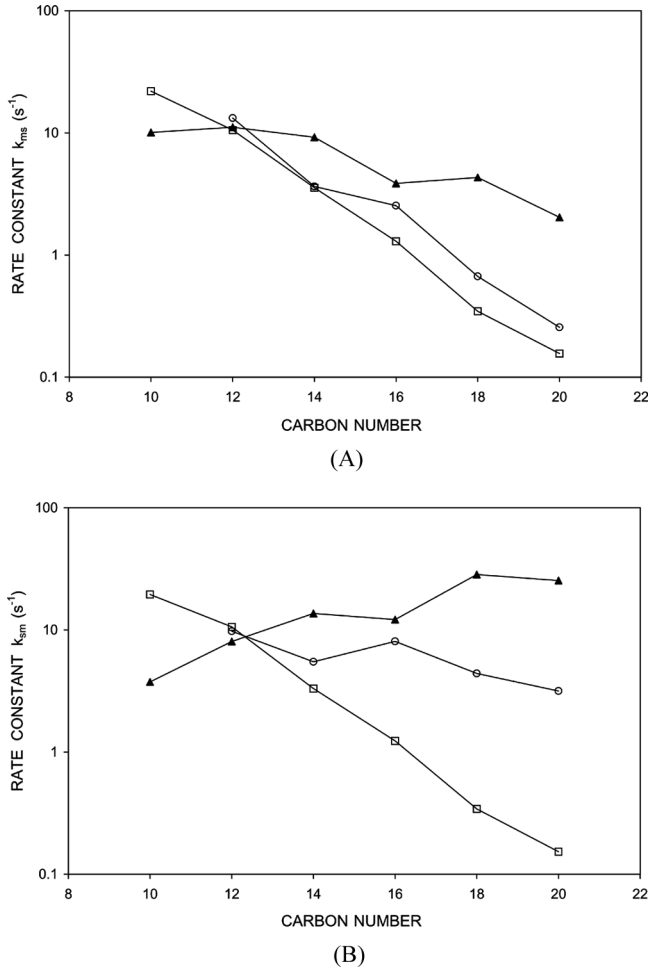

FIGURE 5 Rate constant from stationary to mobile phase (A) and mobile to stationary phase (B) plotted versus carbon number for statistical moment (○), exponentially modified Gaussian (□), and Thomas (▲) methods at 0.088 cm s^{-1}.

factors primarily include the solute affinity for the mobile and stationary phases, diffusion in the stagnant mobile phase layer, diffusion in the stationary phase, and interfacial resistance to mass transfer. Each of these factors is dependent upon the solute carbon number and, hence, will affect the kinetic behavior.

Rate constants for solute transfer from the stationary to mobile phase (k_{ms}) decrease with increasing carbon number. However, the magnitude and rate of change are different for each model. For the statistical moment model, the rate constants for the C_{10} fatty acid could not be determined successfully due to overcorrection, as previously discussed. For the other solutes, the rate constants decrease over two orders of magnitude from C_{12} to C_{20}. The EMG model shows a decrease in rate constant over three orders of magnitude. Rate constants from the moment model are consistently larger than those for the same solute from the EMG model. Rate constants from the Thomas model also decrease with carbon number. However, inconsistencies in this general trend are prevalent throughout the data. That is, the contribution to the rate constant from each additional ethylene unit is relatively constant for both the moment and EMG models, while it is not constant for the Thomas model, as seen in a graph of the logarithm of k_{ms} and k_{sm} versus carbon number (Figure 5A).

Rate constants for solute transfer from the mobile to stationary phase (k_{sm}) decrease with higher carbon number for the moment and EMG models, but increase for the Thomas model. Again, the contribution to the rate constant from each additional ethylene unit is relatively constant for both the moment and EMG models, while it varies for the Thomas model (Figure 5B).

SUMMARY

This study is among the first to compare and support theoretical methods to extract retention factors and kinetic rate constants from experimental data. In this study, the effect of column length, linear velocity, and solute carbon number have been systematically evaluated. Overall, values for the retention factor are similar for each model. Retention factors are constant with distance, decrease with velocity, and increase with solute carbon number. However, the values for the kinetic rate constants differed for each model. The statistical moment and EMG models show the largest variation in rate constant as a function of distance. However, the variation decrease substantially when the rate constants are calculated by difference between two detectors. The moment and EMG methods by difference are more reliable than the Thomas model at one detector. As a function of velocity and solute carbon number, the moment and EMG models show

the most consistent and reliable trends, as compared with the Thomas method. Problems with the Thomas model could be related to the inherent assumptions of the model. The model assumes that broadening arises due to nonlinear isotherms and slow kinetics, and that all column and extra-column effects are negligible. However, due to the nature of the model, extra-column effects cannot be eliminated using the difference approach. Based on these results, the statistical moment and EMG models yield reasonable and consistent values for retention factors and rate constants in an experimental liquid chromatographic system.

ACKNOWLEDGMENTS

The authors thank Dr. Lane C. Sander (National Institute of Standards and Technology) for synthesis of the polymeric octadecyl silica stationary phase and Dr. Shu-Hui Chen for derivatization of the fatty acids.

REFERENCES

1. Giddings, J. C. *Dynamics of Chromatography*, Marcel Dekker: New York, 1965.
2. Miyabe, K.; Guiochon, G. Fundamental Interpretation of the Peak Profiles in Linear Reversed-Phase Liquid Chromatography. *Adv. Chromatogr.* **2000**, *40*, 1–113.
3. Li, X.; Hupp, A. M.; McGuffin, V. L. The Thermodynamic and Kinetic Basis of Liquid Chromatography. *Adv. Chromatogr.* **2007**, *45*, 1–88.
4. Wheeler, J. F.; Beck, T. L.; Klatte, S. J.; Cole, L. A.; Dorsey, J. G. Phase Transitions of Reversed-Phase Stationary Phases: Cause and Effects in the Mechanism of Retention. *J. Chromatogr. A* **1993**, *656*, 317–333.
5. Ranatunga, R. P. J.; Carr, P. W. A Study of the Enthalpy and Entropy Contributions of the Stationary Phase in Reversed-Phase Liquid Chromatography. *Anal. Chem.* **2000**, *72*, 5679–5692.
6. Horvath, C.; Lin, H. J. Movement and Band Spreading of Unsorbed Solutes in Liquid Chromatography. *J. Chromatogr.* **1976**, *126*, 401–420.
7. Horvath, C.; Lin, H. J. Band Spreading in Liquid Chromatography: General Plate Height Equation and a Method for the Evaluation of the Individual Plate Height Contributions. *J. Chromatogr. A* **1978**, *149*, 43–70.
8. Lenhoff, A. M. Significance and Estimation of Chromatographic Parameters. *J. Chromatogr. A* **1987**, *384*, 285–299.
9. Miyabe, K.; Guiochon, G. Measurement of the Parameters of the Mass Transfer Kinetics in High Performance Liquid Chromatography. *J. Sep. Sci.* **2003**, *26*, 155–173.
10. Foley, J. P.; Dorsey, J. G. A Review of the Exponentially Modified Gaussian (EMG) Function: Evaluation and Subsequent Calculation of Universal Data. *J. Chromatogr. Sci.* **1984**, *22*, 40–46.
11. Jeansonne, M. S.; Foley, J. P. Review of the Exponentially Modified Gaussian (EMG) Function Since 1983. *J. Chromatogr. Sci.* **1991**, *29*, 258–266.
12. McGuffin, V. L.; Lee, C. Thermodynamics and Kinetics of Solute Transfer in Reversed-Phase Liquid Chromatography. *J. Chromatogr. A* **2003**, *987*, 3–15.
13. Howerton, S. B.; McGuffin, V. L. Thermodynamic and Kinetic Characterization of Polycyclic Aromatic Hydrocarbons in Reversed-Phase Liquid Chromatography. *Anal. Chem.* **2003**, *75*, 3539–3548.
14. Howerton, S. B.; McGuffin, V. L. Thermodynamics and Kinetics of Solute Transfer in Reversed-Phase Liquid Chromatography: Effect of Annelation in Polycyclic Aromatic Hydrocarbons. *J. Chromatogr.* **2004**, *1030*, 3–12.

15. McGuffin, V. L.; Howerton, S. B.; Li, X. Thermodynamic and Kinetic Characterization of Nitrogen-Containing Polycyclic Aromatic Hydrocarbons in Reversed-Phase Liquid Chromatography. *J. Chromatogr. A* **2005**, *1073*, 63–73.
16. Haarhoff, P. C.; Van der Linde, H. J. Concentration Dependence of Elution Curves in Non-Ideal Gas Chromatography. *Anal. Chem.* **1966**, *38*, 573–582.
17. Wade, J. L.; Bergold, A. F.; Carr, P. W. Theoretical Description of Nonlinear Chromatography with Applications to Physicochemical Measurements in Affinity Chromatography and Implications for Preparative-scale Separations. *Anal. Chem.* **1987**, *59*, 1286–1295.
18. Thomas, H. C. Heterogeneous Ion Exchange in a Flowing System. *J. Am. Chem. Soc.* **1944**, *66*, 1664–1666.
19. Lucy, C. A.; Wade, J. L.; Carr, P. W. Study of Preparative Reversed-Phase Chromatography by Application of Kinetic and Equilibrium Models of Column Overload. *J. Chromatogr. A* **1989**, *484*, 61–82.
20. Hao, W.; Wang, J. Evaluation of Nonlinear Chromatographic Performance by Frontal Analysis using a Simple Multi-Plate Mathematical Model. *J. Chromatogr. A* **2005**, *1063*, 47–56.
21. Cavazzini, A.; Dondi, F.; Jaulmes, A.; Vidal-Madjar, C.; Felinger, A. Monte Carlo Model of Nonlinear Chromatography: Correspondence between the Microscopic Stochastic Model and the Macroscopic Thomas Kinetic Model. *Anal. Chem.* **2002**, *74*, 6269–6278.
22. Jozwiak, K.; Haginaka, J.; Moaddel, R.; Wainer, I. W. Displacement and Nonlinear Chromatographic Techniques in the Investigation of Interaction of Noncompetitive Inhibitors with an Immobilized $\alpha 3\beta 4$ Nicotinic Acetylcholine Receptor Liquid Chromatographic Stationary Phase. *Anal. Chem.* **2002**, *74*, 4618–4624.
23. Li, X.; McGuffin, V. L. Theoretical Evaluation of Methods for Extracting Retention Factors and Kinetic Rate Constants in Liquid Chromatography. *J. Chromatogr. A* **2008**, *1203*, 67–80.
24. van Deemter, J. J.; Zuiderweg, F. J.; Klinkenberg, A. Longitudinal Diffusion and Resistance to Mass Transfer as Causes of Nonideality in Chromatography. *Chem. Eng. Sci.* **1956**, *5*, 271–289.
25. Purnell, H. *Rate Theories of Chromatography*, John Wiley & Sons: New York, 1962; 117–164.
26. Giddings, J. C.; Robinson, R. A. Failure of the Eddy Diffusion Concept of Gas Chromatography. *Anal. Chem.* **1962**, *34*, 885–890.
27. Giddings, J. C. Liquid Chromatography with Operating Conditions Analogous to Those of Gas Chromatography. *Anal. Chem.* **1963**, *35*, 2215–2216.
28. Wilke, C. R.; Chang, P. Correlation of Diffusion Coefficients in Dilute Solutions. *A. I. Ch. E. J.* **1955**, *1*, 264–270.
29. Vidal-Madjar, C.; Guiochon, G. Experimental Characterization of Elution Profiles in Gas Chromatography Using Central Statistical Moments Study of the Relationship Between These Moments and Mass Transfer Kinetics in the Column. *J. Chromatogr.* **1977**, *142*, 61–86.
30. McGuffin, V. L.; Zare, R. N. Laser Fluorescence Detection in Microcolumn Liquid Chromatography: Application to Derivatized Carboxylic Acids. *Appl. Spectrosc.* **1985**, *39*, 847.
31. Evans, C. E.; McGuffin, V. L. Dual On-Column Fluorescence Detection Scheme for Characterization of Chromatographic Peaks. *Anal. Chem.* **1988**, *60*, 573–577.
32. Howerton, S. B.; Lee, C.; McGuffin, V. L. Additivity of Statistical Moments in the Exponentially Modified Gaussian Model of Chromatography. *Anal. Chim. Acta* **2003**, *478*, 99–110.
33. Bujalski, R. *Ph.D. Dissertation*, University of Alberta: Edmonton, 2005.
34. Bujalski, R.; Cantwell, F. F. Measurement of Desorption Rates from Octadecylsilyl Bonded-Phase HPLC Particles and Its Characterization in Terms of Pore, Surface, and Film Diffusion. *Anal. Chem.* **2006**, *78*, 1593–1605.

APPENDIX

Comparison of Various Approaches to the Plate Height Model Using Statistical Moments

As discussed in the text, the statistical moment model accounts for contributions to band broadening from multiple paths, diffusion, and mass

transfer. Accurate estimation of each band broadening term is essential to the model. While the multiple paths (A) and longitudinal diffusion (B_m, B_s) terms are straightforward, a variety of alternative methods have been proposed for the mass transfer contribution to broadening in the mobile phase (C_m). Therefore, in this work, several different methods for determining the mass transfer term, including classical and modern, are evaluated and compared. In this appendix, each method is developed to utilize the difference approach. The difference between two on-column detectors is used to subtract extra-column contributions to broadening.

CLASSICAL KINETIC APPROACHES

As described in the text, the corrected plate height is derived by subtraction of the classical contributions to broadening, such as the A, B_m, B_s, and C_m terms (Equation (9) in text). In this Appendix, the values for A, B_m, and B_s are fixed (Equations (10) to (12)), while those for C_m are compared. That is, the calculated plate heights only differ in their expression for C_m.

The van Deemter[1] form of the mass transfer contribution to plate height in a packed column can be expressed as

$$H_{\text{van Deemter}} = C_m u = \left(\frac{k^2}{100(1+k)^2}\right)\frac{d_p^2 u}{D_m} \tag{A.1}$$

where u is the linear velocity calculated by difference ($u = \Delta L/\Delta t_0$), k is the retention factor calculated by difference (Equation 14), d_p is the particle diameter, and D_m is the diffusion coefficient in the mobile phase.

Based on the model originally developed by Golay[2] for open tubular columns, Purnell[3] developed the following expression for the mass transfer contribution to plate height:

$$H_{\text{Purnell}} = C_m u = \left(\frac{\chi(1+6k+11k^2)}{96(1+k)^2}\right)\frac{d_p^2 u}{D_m} \tag{A.2}$$

where χ is a factor equal to 0.05. In this approach, the packed column is treated as a bundle of open tubes of the same nominal diameter.

An alternative equation was developed by Giddings,[4] in which a single adjustable parameter, ω, is used to represent the first parenthetical term.

$$H_{\text{Giddings}} = C_m u = \omega\frac{d_p^2 u}{D_m} \tag{A.3}$$

Typical values for ω range from 0.5 to 5.

Later, Giddings challenged the idea that each of the sources of broadening is independent and concluded that multiple paths and mass transfer in the mobile phase are coupled to one another.[5] Giddings expressed this coupling as

$$H_{\text{Giddings coupling}} = \left(\frac{1}{A} + \frac{1}{C_m u}\right)^{-1} \tag{A.4}$$

where A is the multiple paths term (Equation 10) and C_m is the Giddings contribution to mobile phase mass transfer (Equation (A.3)).

Each of the mass transfer terms (van Deemter, Purnell, Giddings, and Giddings coupling) can be directly subtracted from the plate height (Equation (9)) in order to obtain the corrected plate height.

MODERN KINETIC APPROACHES

More recently, Miyabe and Guiochon have investigated the individual mass transfer processes that contribute to band broadening.[6] This method does not use the classical expressions for A, B_m, B_s, and C_m. Instead, contributions from axial dispersion, δ_{ax}, external mass transfer, δ_f, and intraparticle diffusion, δ_d, are estimated from the experimental data and used to calculate a corrected plate height.

The sorption equilibrium constant, K, is derived from

$$\frac{\Delta M_1 - \Delta t_0}{1 - \varepsilon} = \left(\frac{\Delta L}{u_s}\right)\rho_p K \tag{A.5}$$

where ε is the interparticle void fraction, ρ_p is the density of the packing material, and u_s is the superficial velocity. In addition, ΔM_1 is the first statistical moment and Δt_0 is the elution time of a non-retained component, both calculated by difference, and ΔL is the distance between detectors. The values for ε and the porosity of the packing material, ε_p, are estimated from Δt_0 using the following equation:

$$\Delta t_0 = \left(\frac{\Delta L}{u_s}\right)(\varepsilon + (1 - \varepsilon)\varepsilon_p) \tag{A.6}$$

The value of K is subsequently obtained from the slope of a plot of the left side of Equation A.5 versus $\Delta L/u_s$. This equilibrium constant is used to characterize the thermodynamic behavior of the system.

The plate height is calculated from

$$H = \left(\frac{\Delta M_2}{(\Delta M_1)^2}\right)\left(\frac{\Delta L}{2u_s}\right) \tag{A.7}$$

where ΔM_2 is the second statistical moment calculated by difference. The contribution from external mass transfer is calculated from

$$\delta_f = (1-\varepsilon)\left(\frac{R_p}{3K_f}\right)(\varepsilon_p + \rho_p K)^2 \tag{A.8}$$

where R_p is the particle radius and k_f is the external mass transfer coefficient. This coefficient is given by

$$k_f = \left(\frac{1.09}{\varepsilon}\right)\left(\frac{\eta}{\rho D_m}\right)^{1/3}\left(\frac{u_s d_p \rho}{\eta}\right)^{1/3}\left(\frac{D_m}{d_p}\right) \tag{A.9}$$

where η and ρ are the viscosity and the density of the mobile phase, respectively. The diffusion coefficient of the solute, D_m, is determined from the Wilke–Chang equation.[7] A dimensionless retention parameter, δ_0, is estimated from Equation A.10 and subsequently used in Equation (A.11) to afford information about the contributions from axial dispersion and intraparticle diffusion.

$$\delta_0 = \varepsilon + (1-\varepsilon)(\varepsilon_p + \rho_p K) \tag{A.10}$$

$$\left(H - \frac{\delta_f}{\delta_0^2}\right) = \left(\frac{D_L}{u_s^2}\right) + \left(\frac{\delta_d}{\delta_0^2}\right) \tag{A.11}$$

From a linear correlation of $(H - \delta_f/\delta_0^2)$ versus $1/u_s$, δ_d can be determined from the intercept. The axial dispersion coefficient, D_L, can be identified from the slope, and subsequently, be used to calculate δ_{ax} as

$$\delta_{ax} = \left(\frac{D_L}{u_s^2}\right)\delta_0^2 \tag{A.12}$$

It should be noted that the value for δ_{ax} is indirectly dependent on the value for δ_f, according to Equation (A.11). Finally, the corrected plate height (ΔH) is calculated by

$$\Delta H = H - \frac{\delta_{ax}}{\delta_0^2} - \frac{\delta_f}{\delta_0^2} - \frac{\delta_d}{\delta_0^2} \tag{A.13}$$

COMPARISON OF PLATE HEIGHT MODELS

In an effort to accurately determine the plate height for the purposes of kinetic measurement, each of the aforementioned models are examined and compared. Representative values for each mass transfer term and the corresponding corrected plate height are given in the following tables with respect to varying solute carbon number and linear velocity. The solutes are coumarin-labeled fatty acids ranging from C_{10} to C_{20}. The linear velocity is varied from 0.045 to 0.368 cm s^{-1}. All other experimental details are given in the text.

As seen in Table A.1, the van Deemter and Purnell contributions to mass transfer are small and similar in magnitude to one another. For both, the contribution increases with increasing carbon number and increasing linear velocity. However, each contribution is 5 orders of magnitude less than the combined contribution from the A, B_m, and B_s terms. Therefore, the subtraction of C_m yields equivalent corrected plate heights for both equations, as seen in Table A.2. Negative values for the corrected plate height indicate overcorrection from the A, B_m, and B_s terms, where the correction is larger than the original plate height. Rate constants cannot be calculated from negative plate heights.

The Giddings mass transfer terms for $\omega = 0.5$ and 5 are summarized in Table A.3. The Giddings correction increases with increasing carbon number and increasing linear velocity. The term is an order of magnitude smaller for $\omega = 0.5$ compared to $\omega = 5$. At $\omega = 5$, the Giddings contribution is the same order of magnitude as the combined contribution from the A, B_m, and B_s terms. This results in overcorrection of the plate height for several solutes, as seen in Table A.4. When ω is decreased to $\omega = 0.5$, the corrected plate height increases, which is due to a smaller correction for the C_m term. Although the Giddings mass transfer term is one order of magnitude lower for $\omega = 0.5$ than $\omega = 5$ (Table A.3), the corrected plate height is relatively similar at the slowest linear velocity (Table A.4). In

TABLE A.1 Mass Transfer Contributions to Plate Height According to van Deemter and Purnell Equations (A.1) and (A.2), Respectively

	$H_{van\ Deemter} = C_m\ u\ (\times 10^{-6}$ cm)		$H_{Purnell} = C_m\ u\ (\times 10^{-6}$ cm)	
Solute	u = 0.045 cm s^{-1}	u = 0.368 cm s^{-1}	u = 0.045 cm s^{-1}	u = 0.368 cm s^{-1}
C_{10}	0.3191	2.181	0.5509	4.232
C_{12}	0.8039	5.419	0.8663	6.464
C_{14}	1.6880	1.134	1.3440	9.823
C_{16}	2.8310	1.983	1.9030	14.110
C_{18}	3.8230	28.180	2.3690	18.090
C_{20}	4.5060	34.620	2.6920	21.130

TABLE A.2 Corrected Plate Height (ΔH) Using van Deemter and Purnell Equations (A.1) and (A.2), Respectively[a]

	ΔH (cm)			
	van Deemter		Purnell	
Solute	$u = 0.045\ cm\ s^{-1}$	$u = 0.368\ cm\ s^{-1}$	$u = 0.045\ cm\ s^{-1}$	$u = 0.368\ cm\ s^{-1}$
C_{10}	−0.0010	0.0032	−0.0010	0.0032
C_{12}	0.0014	0.0035	0.0014	0.0035
C_{14}	0.0059	0.0099	0.0059	0.0099
C_{16}	0.0164	0.0322	0.0164	0.0322
C_{18}	0.0394	0.0375	0.0394	0.0375
C_{20}	0.0477	0.0685	0.0477	0.0686

[a]Values for all other parameters (A, B_m, B_s) as given in text.

TABLE A.3 Mass Transfer Contributions to Plate Height According to Giddings Equation (A.3)

	$H_{Giddings} = C_m\ u\ (\times 10^{-3}\ cm)$			
	$\omega = 5$		$\omega = 0.5$	
Solute	$u = 0.045\ cm\ s^{-1}$	$u = 0.368\ cm\ s^{-1}$	$u = 0.045\ cm\ s^{-1}$	$u = 0.368\ cm\ s^{-1}$
C_{10}	2.046	16.91	0.205	1.691
C_{12}	2.169	17.93	0.217	1.793
C_{14}	2.286	18.89	0.229	1.889
C_{16}	2.401	19.84	0.240	1.984
C_{18}	2.510	20.74	0.251	2.074
C_{20}	2.616	21.61	0.262	2.161

TABLE A.4 Corrected Plate Height (ΔH) Using Giddings Equation (A.3)[a]

	ΔH (cm)			
	Giddings, $\omega = 5$		Giddings, $\omega = 0.5$	
Solute	$u = 0.045\ cm\ s^{-1}$	$u = 0.368\ cm\ s^{-1}$	$u = 0.045\ cm\ s^{-1}$	$u = 0.368\ cm\ s^{-1}$
C_{10}	−0.0030	−0.0136	−0.0012	0.0016
C_{12}	−0.0008	−0.0144	0.0012	0.0017
C_{14}	0.0037	−0.0090	0.0057	0.0080
C_{16}	0.0140	0.0124	0.0162	0.0303
C_{18}	0.0370	0.0168	0.0392	0.0355
C_{20}	0.0451	0.0470	0.0474	0.0664

[a]Values for all other parameters (A, B_m, B_s) as given in text.

contrast, at the fastest linear velocity, the corrected plate heights for the two values of ω are substantially different. At the slowest linear velocity, the corrected plate heights for the Giddings equation for both values of ω are similar in magnitude to those calculated using the van Deemter and Purnell equations (Table A.2). However, at the fastest linear velocity, only the corrected plate heights for the Giddings model for $\omega = 0.5$ are similar to those calculated using the other models. Since ω represents the retention factor dependence of the mass transfer term, a value of 0.5 appears to be more similar to the k dependence of the van Deemter and Purnell equations.

The values for the Giddings coupling contribution calculated using Equation (A.4) are summarized in Table A.5. These values are a combination of the contribution from both A and C_m terms. Values for the Giddings coupling contribution increase with increasing carbon number and increasing linear velocity. The term is smaller for $\omega = 0.5$ compared to $\omega = 5$. The corrected plate heights for the Giddings coupling method are summarized in Table A.6. The coupling method yields no negative or overcorrected plate heights. However, the plate heights for the Giddings coupling method are approximately half the magnitude of those from the van Deemter and Purnell equations.

The modern method advocated by Miyabe and Guiochon,[6] summarized in Equations A.5 to A.13, is quite different from the classical approach to the plate height model. Values for the corrected plate height are shown in Table A.7. The corrected plate height increases with increasing carbon number yet, in contrast to the classical models, decreases with increasing linear velocity. Corrected plate heights for the Guiochon method are one to two orders of magnitude larger than those from the classical models. Some overcorrection, primarily due to axial dispersion, is still observed for narrow peaks. The parameters in this method are determined from the flow rate, rather than the linear velocity ($\Delta L/\Delta t_0$), and thus error may arise from inaccuracies in the flow rate measurement.

TABLE A.5 Mass Transfer Contributions to Plate Height According to Giddings Coupling Equation (A.4)

	$H_{\text{Giddings coupling}} = C_m\ u\ (\times 10^{-3}\,\text{cm})$			
	$\omega = 5$		$\omega = 0.5$	
Solute	$u = 0.045\,\text{cm s}^{-1}$	$u = 0.368\,\text{cm s}^{-1}$	$u = 0.045\,\text{cm s}^{-1}$	$u = 0.368\,\text{cm s}^{-1}$
C_{10}	0.7154	1.033	0.1725	0.6664
C_{12}	0.7299	1.036	0.1812	0.6817
C_{14}	0.7426	1.039	0.1893	0.6951
C_{16}	0.7544	1.042	0.1971	0.7076
C_{18}	0.7648	1.044	0.2044	0.7187
C_{20}	0.7744	1.046	0.2113	0.7289

TABLE A.6 Corrected Plate Height (ΔH) Using Giddings Coupling Equation (A.4)[a]

	ΔH (cm)			
	Giddings coupling, $\omega = 5$		Giddings coupling, $\omega = 0.5$	
Solute	$u = 0.045\ cm\ s^{-1}$	$u = 0.368\ cm\ s^{-1}$	$u = 0.045\ cm\ s^{-1}$	$u = 0.368\ cm\ s^{-1}$
C_{10}	0.0000	0.0008	0.0005	0.0012
C_{12}	0.0009	0.0009	0.0015	0.0013
C_{14}	0.0029	0.0035	0.0034	0.0038
C_{16}	0.0074	0.0122	0.0080	0.0126
C_{18}	0.0178	0.0141	0.0183	0.0144
C_{20}	0.0214	0.0255	0.0219	0.0259

[a]Values for all other parameters (A, B_m, B_s) as given in text.

It is important to note that most of the methods examined herein yield comparable values for the corrected plate height and, hence, comparable kinetic rate constants. However, the number of variables and the accuracy with which they are known can limit the accuracy of each method. The van Deemter equation is straightforward, having no adjustable parameters. The Purnell equation generates comparable values to the van Deemter equation, however, it relies on a proportionality constant (χ) that dictates the magnitude of the mass transfer term. While the Giddings mass transfer equation is straightforward, it also relies on a proportionality constant (ω). Depending upon the magnitude of this constant, it can cause an overcorrection in the plate height for some solutes at some flow rates, making it less useful in practice. The Giddings coupling theory, with a similar adjustable parameter, provides corrected plate heights that are approximately half the magnitude of the other classical models. On the other hand, the Guiochon method yields corrected plate heights that are substantially larger than those from the classical methods. This method is more

TABLE A.7 Corrected Plate Height (ΔH) Using Modern Kinetic Method of Guiochon (Equation (A.13))

	ΔH (cm)	
	Guiochon	
Solute	$u = 0.045\ cm\ s^{-1}$	$u = 0.368\ cm\ s^{-1}$
C_{10}	−0.0270	0.0046
C_{12}	0.0210	0.0023
C_{14}	0.1395	0.0204
C_{16}	0.3774	0.1003
C_{18}	0.8572	0.1101
C_{20}	1.0181	0.2028

challenging to use, as it relies on experimentally derived values for numerous variables. Thus, after investigation of each method, the van Deemter equation is deemed most suitable for these chromatographic conditions and, thus, is selected for primary use in this study.

REFERENCES

1. van Deemter, J. J.; Zuiderweg, F. J.; Klinkenberg, A. Longitudinal Diffusion and Resistance to Mass Transfer as Causes of Nonideality in Chromatography. *Chem. Eng. Sci.* **1956**, *5*, 271–289.
2. Golay, M. J. E. *Gas Chromatography*; Butterworths: London, **1958**.
3. Perrett, R. H.; Purnell, J. H. Contribution of Diffusion and Mass Transfer Processes to Efficiency of Gas Liquid Chromatography Columns. *Anal. Chem.* **1963**, *35*, 430–439.
4. Giddings, J. C. *Dynamics of Chromatography*, Marcel Dekker: New York, **1965**.
5. Giddings, J. C. Eddy Diffusion in Chromatography. *Nature* **1960**, *187*, 1023–1024.
6. Miyabe, K.; Guiochon, G. Measurement of the Parameters of the Mass Transfer Kinetics in High Performance Liquid Chromatography. *J. Sep. Sci.* **2003**, *26*, 155–173.
7. Wilke, C. R.; Chang, P. Correlation of Diffusion Coefficients in Dilute Solutions. *A. I. Ch. E. J.* **1955**, *1*, 264–270.